AMERICAN SOCIETY FOR MICROBIOLOGY | Journal of Virology®

VIRUS-CELL INTERACTIONS

Neuropilin-1 Facilitates Pseudorabies Virus Replication and Viral Glycoprotein B Promotes Its Degradation in a Furin-Dependent Manner

Meng Chen,[a] Meng-Hang Wang,[a] Xue-Gang Shen,[a] Hao Liu,[b] Yu-Yuan Zhang,[a] Jin-Mei Peng,[a] Fandan Meng,[a] Tong-Yun Wang,[a] Yuan-Zhe Bai,[a] Ming-Xia Sun,[a] Zhi-Jun Tian,[a] Xin Yin,[a] Xue-Hui Cai,[a,c] Yan-Dong Tang[a,c]

[a]State Key Laboratory of Veterinary Biotechnology, Harbin Veterinary Research Institute of Chinese Academy of Agricultural Sciences, Harbin, China
[b]School of Life Sciences and Engineering, Foshan University, Foshan, Guangdong Province, China
[c]Heilongjiang Provincial Key Laboratory of Veterinary Immunology, Harbin, China

Meng Chen and Meng-Hang Wang contributed equally to this work. Meng Chen located the phenotype and both authors performed most of the experiments.

ABSTRACT Pseudorabies virus (PRV), which is extremely infectious and can infect numerous mammals, has a risk of spillover into humans. Virus–host interactions determine viral entry and spreading. Here, we showed that neuropilin-1 (NRP1) significantly potentiates PRV infection. Mechanistically, NRP1 promoted PRV attachment and entry, and enhanced cell-to-cell fusion mediated by viral glycoprotein B (gB), gD, gH, and gL. Furthermore, through *in vitro* coimmunoprecipitation (Co-IP) and bimolecular fluorescence complementation (BiFC) assays, NRP1 was found to physically interact with gB, gD, and gH, and these interactions were C-end Rule (CendR) motif independent, in contrast to currently known viruses. Remarkably, we illustrated that the viral protein gB promotes NRP1 degradation via a lysosome-dependent pathway. We further demonstrate that gB promotes NRP1 degradation in a furin-cleavage-dependent manner. Interestingly, in this study, we generated gB furin cleavage site (FCS)-knockout PRV (Δfurin PRV) and evaluated its pathogenesis; *in vivo*, we found that Δfurin PRV virulence was significantly attenuated in mice. Together, our findings demonstrated that NRP1 is an important host factor for PRV and that NRP1 may be a potential target for antiviral intervention.

IMPORTANCE Recent studies have shown accelerated PRV cross-species spillover and that PRV poses a potential threat to humans. PRV infection in humans always manifests as a high fever, tonic-clonic seizures, and encephalitis. Therefore, understanding the interaction between PRV and host factors may contribute to the development of new antiviral strategies against PRV. NRP1 has been demonstrated to be a receptor for several viruses that harbor CendR, including SARS-CoV-2. However, the relationships between NRP1 and PRV are poorly understood. Here, we found that NRP1 significantly potentiated PRV infection by promoting PRV attachment and enhanced cell-to-cell fusion. For the first time, we demonstrated that gB promotes NRP1 degradation via a lysosome-dependent pathway. Last, *in vivo*, Δfurin PRV virulence was significantly attenuated in mice. Therefore, NRP1 is an important host factor for PRV, and NRP1 may be a potential target for antiviral drug development.

KEYWORDS pseudorabies virus, neuropilin-1, entry, C-end Rule, glycoprotein B, virulence, pathogenesis

Pseudorabies virus (PRV) belongs to the alphaherpesvirus subfamily of herpesviruses (1, 2). Pigs are the only natural host for PRV, but the virus can naturally infect a wide range of host mammals (3, 4). Recent studies have shown accelerated PRV cross-species

Editor Lori Frappier, University of Toronto

Address correspondence to Yan-Dong Tang, tangyandong2008@163.com, Xue-Hui Cai, caixuehui139@163.com, or Xin Yin, yinxin@caas.cn.
The authors declare no conflict of interest.
Received 22 August 2022
Accepted 16 September 2022
Published 29 September 2022

spillover, making PRV a potential threat to humans. PRV is extremely infectious, and infected pigs shed large quantities of virus in bodily secretions and excretions (5–8). Therefore, understanding the interaction between PRV and host factors may contribute to the development of new antiviral strategies.

To establish successful infection, PRV must first attach to cell receptors and then enter the cell to release its genetic material. In this process, PRV glycoproteins, including glycoprotein B (gB), gC, gD, and gH/gL, play a central role in viral attachment, entry, and cell-to-cell spread (9–12). PRV gB is the most conserved envelope glycoprotein of herpesviruses, and the gB proteins from PRV and herpes simplex virus 1 (HSV-1) share 50% amino acid sequence identity (10, 13). However, in contrast with HSV-1 gB, PRV gB contains a consensus furin cleavage site (FCS), "RRARR," which can be cleaved by ubiquitously expressed furin in most cells (13–15). Thus, gB exists as three glycoproteins, gBa, gBb, and gBc; the gBb and gBc subunits are the cleavage products of gBa (16). Furin is a well-known host factor that determines the pathogenesis of some viruses, such as influenza virus subtypes H5 and H7 and SARS-CoV-2 (17–21). However, the role of furin in PRV pathogenesis has not been fully investigated. Furin cleaves FCS to generate a carboxy-terminal RXXR sequence, which is also known as the C-end Rule or CendR motif (17). Multiple molecules, such as transforming growth factor β, vascular endothelial growth factor (VEGF)-A isoform, VEGF-A165, and semaphorin 3A (Sema3A), harbor the CendR motif (22). The C-terminal CendR motifs in these molecules possess the strong ability to interact with the b1 domain of neuropilin-1 (NRP-1) and initiate cellular internalization and vascular permeability (17, 23).

NRP1 is a cell-surface receptor that plays an essential role in angiogenesis, immune function, viral entry, the regulation of vascular permeability, and the development of the nervous system (23). NRP1 is also a key host factor required for various viruses harboring the CendR motif; however, the roles of NRP1 in distinct viruses may be controversial. For the herpesvirus Epstein–Barr virus (EBV) (24), SARS-CoV-2 (25–27), the retroviruses human T-cell lymphotropic virus-1 (HTLV-1) and HTLV-2 (28, 29), and mouse cytomegalovirus (mCMV) (30), NRP1 acts as a cellular (co)receptor and could significantly promote virus replication. However, for human immunodeficiency virus-1 (HIV-1), NRP1 serves as a host restriction factor that inhibits HIV-1 replication (31).

Given the apparent importance of NRP1 in viral replication and the fact that PRV harbors the CendR motif, we aimed to study the role of NRP1 in the life cycle of PRV. Our findings showed NRP1 overexpression increased PRV attachment and promoted viral glycoprotein-mediated cell-to-cell fusion. Through coimmunoprecipitation (Co-IP) and bimolecular fluorescence complementation (BiFC) assays, we also illustrated that NRP1 physically interacts with gB, gD, and gH, and that this interaction is CendR motif independent. Furthermore, we found that gB promotes NRP1 degradation via a lysosome-dependent pathway and that this degradation is dependent on the cleavage of gB by furin. Lastly, we also evaluated the pathogenesis of Δfurin PRV *in vivo* and found that this genetically modified PRV was significantly attenuated in mice.

RESULTS

NRP1 is a host factor that promotes PRV infection. To investigate the role of NRP1 in PRV replication, RK13 cells were transfected with NRP1 or a control and then infected with EGFP reporter PRV (32) at a multiplicity of infection (MOI) of 0.1. Twenty-four hours later, we observed more PRV-induced cytopathic effects in NRP1-transfected cells (Fig. 1A). The expression of NRP1 was confirmed by Western blotting (Fig. 1B). In addition, the production of PRV in the supernatant was measured, and our results demonstrated that NRP1 significantly promoted PRV replication (~9-fold) in RK13 cells (Fig. 1B). We further confirmed this result in HEK293T cells and Vero-E6 cells (Fig. 1C and D). Next, we evaluated the role of endogenous NRP1 in PRV replication. Because we failed to detect endogenous NRP1 expression in RK13 cells, HEK293T cells, or Vero-E6 cells (data not shown), we used an NRP1-expressing human neuroblastoma cell line, SK-N-SH, to perform an RNA interference assay. Three potential siRNAs were screened,

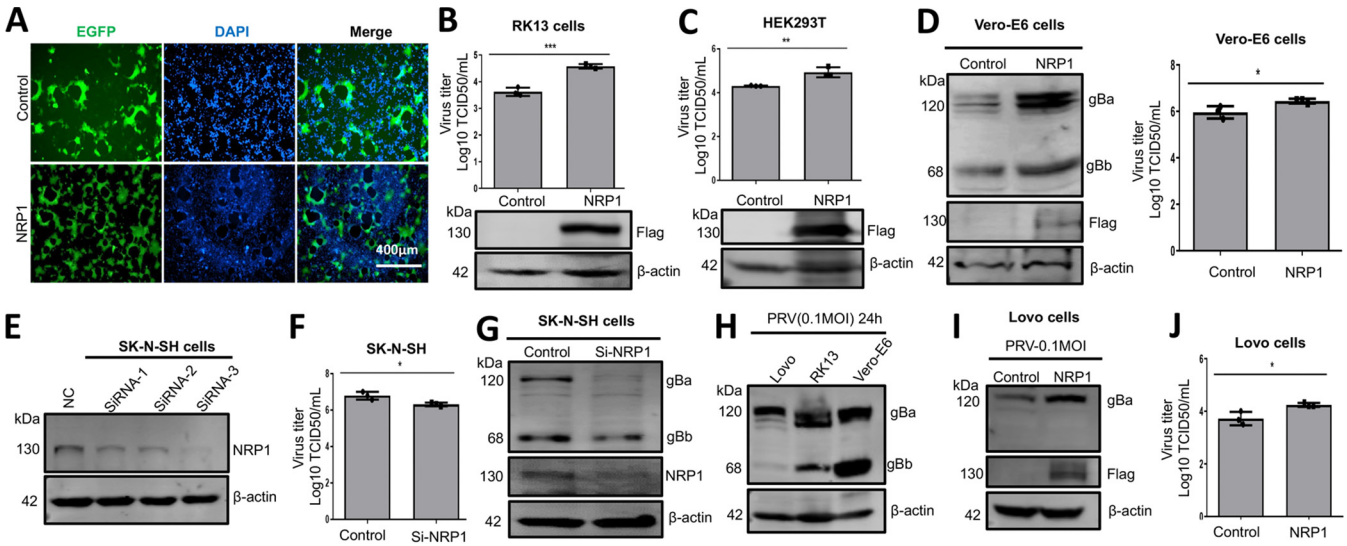

FIG 1 NRP1 promotes PRV proliferation. (A) RK13 cells were transfected with 1 μg control or p-Flag-NRP1 plasmid in 12-well plates for 24 h and then infected with PRV-GFP at an MOI of 0.1. After 24 h, the cells were observed under a fluorescence microscope. Scale bars, 400 μm. (B) The supernatant in (A) was collected at 24 h for a TCID50 assay in Vero-E6 cells, and cell lysates were collected for Western blotting. (C) HEK293T cells were transfected with 1 μg control or p-Flag-NRP1 plasmid for 24 h in 12-well plates and then infected with PRV at an MOI of 0.1 for 24 h. The PRV titer in the supernatants was measured with a TCID50 assay, and the cells were collected for Western blotting. (D) Vero-E6 cells were transfected with 1 μg control or p-Flag-NRP1 plasmid in 12-well plates for 24 h and then infected with PRV-GFP at an MOI of 0.1, after which the cells were lysed at 24-hpi. gB expression in the cells was detected by Western blotting (left). The supernatant was collected at 24 h for a TCID50 assay in Vero-E6 cells (right). (E) SK-N-SH cells were transfected with siRNA targeting NRP1 or negative control (NC) at a final concentration of 60 nM in 12-well plates, and 48 h after transfection, NRP1 expression was detected by Western blotting. (F) SK-N-SH cells were transfected with NRP1 or control siRNA at a final concentration of 60 nM and then infected with PRV at an MOI of 0.1. After 48 h of transfection, the PRV titer in the supernatants was measured with a TCID50 assay. (G) After transfection with control or siRNA-3 against NRP1 at a final concentration of 60 nM in 24-well plates for 48 h, SK-N-SH cells were treated with PRV at an MOI of 0.1 for 48 h. The level of gB in the cells was detected by Western blotting. (H) LoVo, RK13, and Vero-E6 cells were infected with PRV (MOI of 0.1) for 24 h in 12-well plates. The cells were then harvested to detect the gB level via Western blotting. (I) LoVo cells were transfected with 1 μg control or p-Flag-NRP1 plasmid in 12-well plates for 24 h, and then, the cells were infected with PRV at an MOI of 0.1 for 24 h. The level of gB in the cells was detected by Western blotting. (J) The 24-h cell supernatant in (I) was collected for a TCID50 assay in Vero-E6 cells. The values in all graphs are the means $\pm$ SD. ***, $P < 0.001$; **, $P < 0.01$; *, $P < 0.05$; Student's *t* test.

and the endogenous expression of NRP1 in SK-N-SH cells was efficiently knocked down by siRNA-3 (Fig. 1E). Therefore, we used this siRNA in subsequent experiments. In SK-N-SH cells, NRP1 knockdown significantly decreased PRV titers and viral protein expression (Fig. 1F and G). NRP1 was reported to promote the replication of several viruses in a CendR motif-dependent manner (17). Here, we tested whether NRP1 promotes PRV replication in a CendR-dependent manner. We used human colon carcinoma LoVo cells, which lack endogenous furin; therefore, gB would not be cleaved in this cell line (15). We verified that LoVo cells failed to cleave gB; in contrast, gB was efficiently cleaved by furin in RK13 cells and Vero cells (Fig. 1H). Interestingly, NRP1 also significantly enhanced the expression of gB and promoted PRV replication in LoVo cells transfected with NRP1 (Fig. 1I and J). These results suggested that NRP1 may promote PRV replication through a CendR motif-independent pathway, in contrast to other reported viruses.

NRP1 promotes PRV entry by approximately 2-fold. Because NRP1 is known to serve as an entry receptor for several viruses, we next tested whether NPR1 is a potential PRV entry receptor. Chinese hamster ovary (CHO) cells are resistant to PRV entry due to the absence of entry receptors (33). Therefore, we used CHO cells to investigate PRV entry. CHO cells were transfected with NRP1 or a control, and Nectin-1 (an identified PRV entry receptor) was used as a positive control. Twenty-four hours later, the transfected cells were infected with rPRVTJ-NLuc expressing NanoLuc luciferase (34). Six-hours postinfection (hpi), the infected cells were lysed, and NanoLuc luciferase activity was detected. We found that Nectin-1 expression could enhance PRV entry into CHO cells, as NanoLuc luciferase activity was approximately 23-fold higher than that in the control. In contrast, NanoLuc luciferase activity in the NRP1-transfected cells was

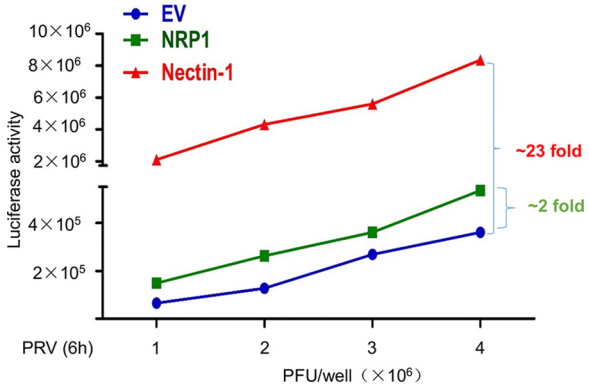

FIG 2 NRP1 promotes PRV entry by 2-fold. CHO cells were transfected with 0.5 μg plasmids to induce expression of p-Flag-NRP1, p-Nectin-1, or control in 24-well plates. After 24 h, the transfected cells were infected with rPRVTJ-NLuc (1~4 $\times$ 10^6 PFU/well). Six hours after inoculation, the cells were lysed and assayed with a Nano-Glo Luciferase Assay System.

approximately 2-fold higher than that in the control (Fig. 2). Therefore, NRP1 moderately promotes PRV entry, and may not be as effective as Nectin-1.

NRP1 enhanced PRV attachment and viral glycoprotein- (gB-, gD-, gH-, and gL-) mediated cell-to-cell fusion. As shown above, NRP1 promotes PRV replication, and thus, we wanted to investigate which step(s) in the PRV life cycle are regulated by NRP1. NRP1 is a cell surface localized protein; therefore, we first evaluated the PRV attachment stage and the viral glycoprotein-mediated cell-to-cell fusion stage because these steps occur in the cell membrane. We first tested whether NRP1 could promote PRV attachment. We inoculated HEK293T and CHO cells with PRV at an MOI of 1, allowed the viruses to attach to the cells at 4°C for 2 h, and then washed the cells three times with cold PBS. Viral DNA was extracted and quantified with real-time PCR, and we found that PRV attachment in NRP1-transfected cells was significantly higher than in control cells (Fig. 3A and B). Next, we evaluated the role of endogenous NRP1 in PRV attachment in two neuronal cell lines: SK-N-SH and SH-SY5Y. We found that knockdown of endogenous NRP1 in these cell lines significantly decreased virus attachment (Fig. 3C and D). These data collectively suggested that NRP1 enhanced PRV attachment.

Next, we tested whether cell-to-cell fusion is regulated by NRP1. PRV-mediated cell-to-cell fusion requires the glycoproteins gB, gD, gH, and gL. We performed a cell-to-cell fusion assay via cotransfection of RK13 cells with NRP1 or a control plasmid and with the gB, gD, gL, gH, and pDC315-EGFP plasmids. The results indicated that the NRP1-transfected group formed larger syncytia (Fig. 4A). Fusion activity was calculated based on the relative EGFP area, which was analyzed using ImageJ. The results demonstrated that NRP1 significantly promoted viral glycoprotein-mediated cell-to-cell fusion (Fig. 4B). We further confirmed this result in HEK293T cells (Fig. 4C and D). We also used a luciferase reporter system to evaluate viral glycoprotein-mediated cell-to-cell fusion in HEK293T cells, as illustrated in Fig. 4E. HEK293T effector cells transfected with the PGL5-Luc plasmid were mixed with HEK293T target cells cotransfected with pBind-Id and PACT-Myod plasmids. Twelve hours later, the mixed cells were cotransfected with an NRP1 or control plasmid and the gB, gD, gL, and gH plasmids. Viral glycoprotein-mediated cell-to-cell fusion was quantified based on the luciferase activities in cell lysates at 48-h posttransfection. The results indicated that NRP1 significantly increased viral glycoprotein-mediated cell-to-cell fusion activity (Fig. 4F).

NRP1 interacted with gB, gD, and gH, but not gL. We demonstrated that NRP1 efficiently promoted PRV attachment and viral glycoprotein-mediated cell-to-cell fusion. However, the detailed mechanism remains unclear. Because gB can be cleaved by furin, a CendR motif that is known to interact with NRP1 was generated. Next, we detected whether NRP1 interacted with gB. HEK293T cells were transfected with gB expression plasmids with the NRP1 plasmid or a control plasmid. By a coimmunoprecipitation assay,

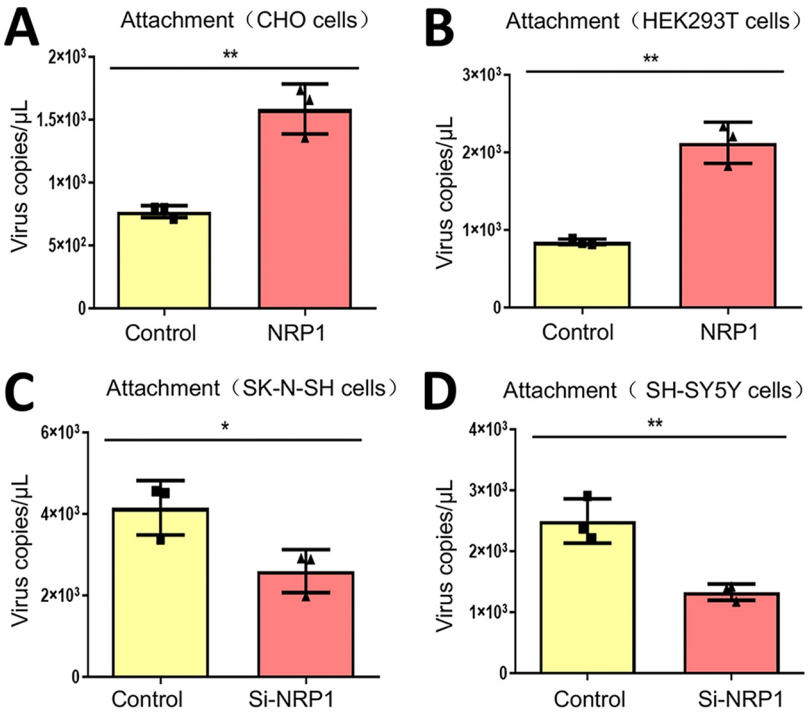

FIG 3 NRP1 facilitates PRV attachment. (A) CHO and (B) HEK293T cells were transfected with 1 μg control or p-Flag-NRP1 plasmid in 12-well plates for 24 h and then infected with PRV at an MOI of 1 and maintained at 4°C. Two hours later, the cells were washed three times with cold PBS, and DNA was extracted and quantified via qPCR. (C) SK-N-SH and (D) SH-SY5Y cells were plated in 24-well plates and transfected with siRNA-3 or control at a final concentration of 60 nM. After 48 h, the cells were infected with PRV at an MOI of 1 and then maintained at 4°C. Two hours later, the cells were subjected to attachment assays. The values in graphs are the means ± SD. **, $P < 0.01$; *, $P < 0.05$; Student's *t* test.

we demonstrated that NRP1 interacted with gB (Fig. 5A). We further investigated whether NRP1 interacted with other glycoproteins. Interestingly, we found that NRP1 also interacted with gD and gH, which lack the CendR motif (Fig. 5B and C). However, we did not detect any interaction between NRP1 and gL (Fig. 5D). To further confirm these interactions, we performed a BiFC assay, which has been extensively applied to study protein-protein interactions (35, 36). HEK293T cells were cotransfected with the plasmids, including pVC-gB, pVC-gD, pVC-gH, or pVC-gL and pVN-NRP1 to detect protein-protein interactions. As expected, we obtained the same results as observed in the Co-IP assay; NRP1 interacted well with gB, gD, and gH but not with gL (Fig. 5E). Using an anti-gB antibody, we further verified whether the PRV gB protein interacts with endogenous NRP1. In SH-SY5Y cells, through IP with endogenous NRP1, we detected an interaction between NRP1 and gB protein (Fig. 5F). Because we did not have an anti-gD or anti-gH antibody, we were not able to further confirm the interaction between these proteins and endogenous NRP1. Therefore, NRP1 promoted PRV attachment and viral glycoprotein-mediated cell-to-cell fusion, potentially through interactions with PRV gB, gD, and gH.

gB promotes NRP1 degradation via lysosomal-dependent pathways. Interestingly, by evaluating the interactions between NRP1 and viral glycoproteins, we found that NRP1 could be specifically downregulated by gB but not by gD, gH, or gL (Fig. 6A). Additionally, gB decreased NRP1 expression in a dose-dependent manner (Fig. 6B). We hypothesized that gB may promote NRP1 degradation via the ubiquitin–proteasome-dependent pathway or the lysosome-dependent pathway. We used two inhibitors, chloroquine (CQ, a lysosome pathway inhibitor) and MG132 (a ubiquitin–proteasome inhibitor), to evaluate which pathway was involved in NPR1 degradation. The results showed that the lysosome pathway inhibitor CQ but not MG132 reversed the degradation of NRP1 (Fig. 6C). This result indicated that PRV gB promoted NRP1 degradation

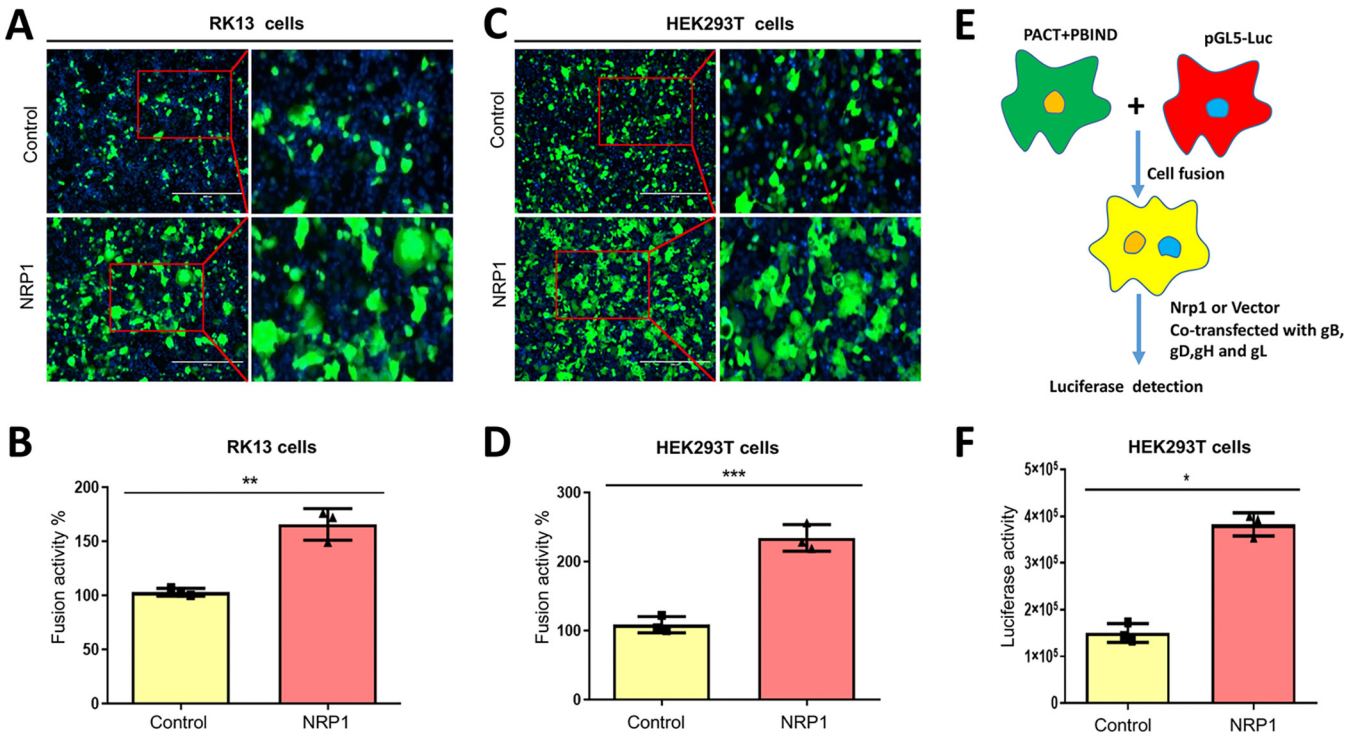

FIG 4 NRP1 promotes viral protein-mediated cell-to-cell membrane fusion. (A) RK13 and (C) HEK293T cells were cotransfected with 500 ng p-Flag-NRP1 or control plasmid, with 200 ng pDC315-EGFP, and with 125 ng pCAGGS-HA-gB, pCAGGS-HA-gD, pCAGGS-HA-GI, or pCAGGS-HA-gH in 12-well plates. Thirty-six hours after transfection, the cells were observed by fluorescence microscopy. (B) The relative GFP area in RK13 cells and (D) HEK293T cells was analyzed with ImageJ. The relative GFP area in the control group was set to 100%. (E) Schematic showing the fusion assay. When HEK293T cells grew to 90% confluence in a 6-well plate, the cells were cotransfected with 2 μg pBind-Id and 2 μg PACT-Myod plasmids and mixed with other HEK293T cells transfected with 0.5 μg PGL5-Luc plasmid. Then, the cells were replated in 48-well plates, and 12 h later, the cells were cotransfected with 125 ng p-Flag-NRP1 or control and with 32 ng pCAGGS-HA-gB, 32 ng pCAGGS-HA-gD, 32 ng pCAGGS-HA-gL, or 32 ng pCAGGS-HA-gH. (F) Forty-eight hours later, the cells were lysed, and cell-to-cell membrane fusion was evaluated via luciferase activity. Error bars indicate the standard deviation (SD); ***, $P < 0.001$; **, $P < 0.01$; *, $P < 0.05$.

via the lysosome pathway. We further confirmed these results in RK13 cells (Fig. 6D and E). We next evaluated whether PRV infection could promote the degradation of endogenous NRP1. SH-SY-5Y cells were infected with PRV, and we found that endogenous NRP1 was degraded when PRV infection was present, but this degradation was reversed by CQ (Fig. 6F). These results demonstrated that gB specifically promoted NRP1 degradation via a lysosomal-dependent pathway.

gB-promoted NRP1 degradation was dependent on furin cleavage. We demonstrated that NRP1 promoted PRV replication independent of the gB CendR motif (Fig. 1I). Here, we wanted to evaluate whether NRP1 degradation was gB CendR motif dependent. We attempted to construct several gB mutants, including gB-Δ500R, gB-Δ500-501RA, and gB-Δfurin, to block gB cleavage by furin (Fig. 7A). After transfection, we found that the Δ500R construct could be cleaved by furin, like wild-type gB; however, the Δ500-501 RA and Δfurin constructs of PRV gB failed to be cleaved by furin (Fig. 7B). We next tested whether these findings indicate that PRV gB mutants could promote NRP1 degradation. We cotransfected NRP1 with the indicated gB mutants into HEK293T cells. The results showed that the Δ500-501RA and Δfurin constructs failed to degrade NRP1, similar to wild-type gB, which demonstrated that NRP1 degradation was gB CendR motif dependent (Fig. 7C). However, NRP1 could also interact with these constructs, indicating that the interaction between NRP1 and gB was CendR motif independent (Fig. 7C).

NRP1 promoted PRV replication via a CendR-independent pathway. We next tested whether NRP1 promoted PRV replication in a CendR-dependent manner during PRV infection. We generated the indicated gB mutants of PRV via CRISPR/Cas9 technology, as previously described (37). PRV gB-Δ500R, PRV gB-Δ500-501RA, and PRV gB-

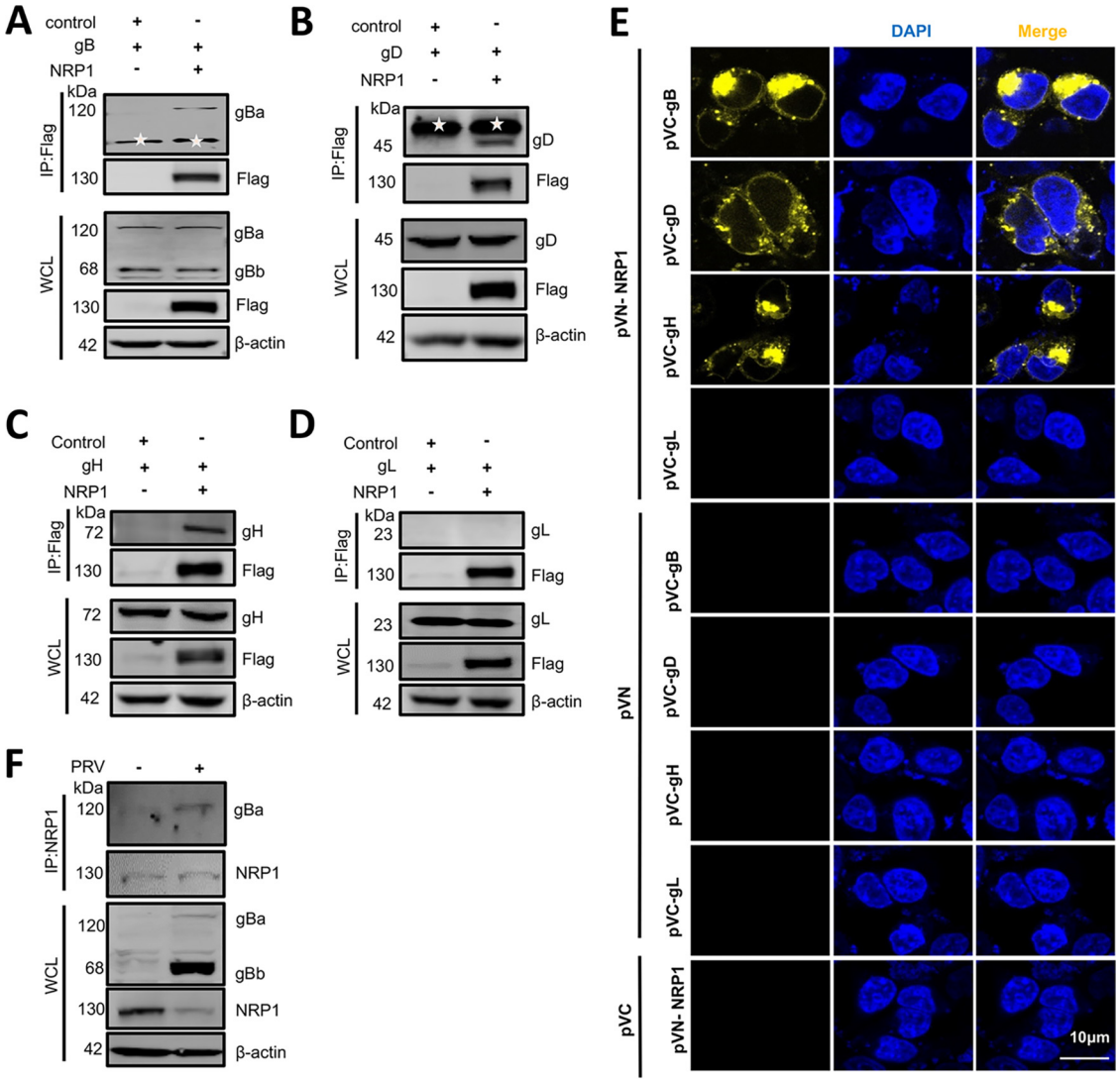

FIG 5 NRP1 interacts with PRV-gB, PRV-gD, and PRV-gH but not with PRV-gL. (A) HEK293T cells grown to approximately 70% to 80% confluence in 6-well plates were cotransfected with 1.5 μg p-Flag-NRP1 or control plasmids and 1.5 μg pCAGGS-HA-gB, (B) pCAGGS-HA-gD, (C) pCAGGS-HA-gL, or (D) pCAGGS-HA-gH for 24 h. Then, the cells were immunoprecipitated (IP) with an antibody against Flag, followed by immunoblotting (IB) analysis for the complex with the indicated antibody. Star labeled band indicated as heavy chain of antibodies. (E) Imaging of the gB, gD, gH, and gL interaction with NRP1 using the bimolecular fluorescence complementation system (BiFC). HEK293T cells were cotransfected with the indicated vectors under normal conditions. In the BiFC system, interacting proteins are shown in yellow, and the nuclei were stained with DAPI. Images were acquired using confocal microscopy under a 63× lens objective. Appearance of yellow fluorescence represents a positive observation; the images were selected and cropped to show the positive results. (F) SH-SY5Y cells grown to approximately 90% confluence in 6-well plates were infected with PRV (MOI of 0.1) for 24 h. Then, the cells were immunoprecipitated (IP) with an antibody against NRP1, followed by immunoblotting (IB) analysis for the complex with the indicated antibody.

Δfurin were successfully generated and confirmed by DNA sequencing (data not shown). We next infected cells with the indicated PRV mutants and found that the gB proteins of wild-type PRV and Δ500R PRV could be successfully cleaved by furin; however, very little gB from Δ500-501RA PRV and Δfurin PRV was cleaved (Fig. 8A). Interestingly, the plaque sizes of these gB-modified PRV constructs were not different from that of wild-type PRV in both Vero cells and swine testicle (ST) cells (Fig. 8B). In addition, no significant differences were observed in the replicative kinetics of gB-modified PRV compared with wild-type PRV in Vero cells and HEK293T cells (Fig. 8C and D). Finally, we evaluated whether the replication of these FCS-modified PRVs could be promoted by NPR1 during PRV infection and found that the production of all these viruses was promoted by NRP1 (Fig. 8E).

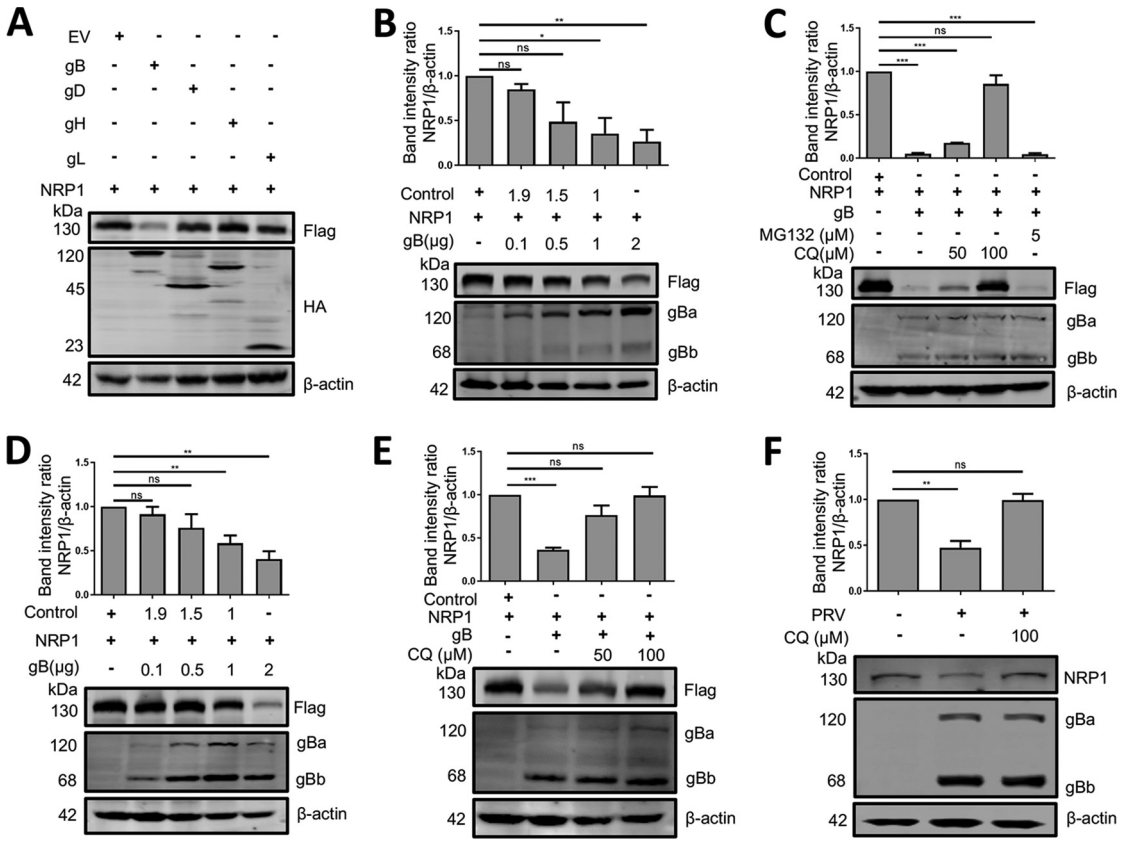

FIG 6 PRV employs gB to decrease NRP1 in a lysosomal-dependent degradation pathway. (A) HEK293T cells were cotransfected with 0.5 μg p-Flag-NRP1 and 0.5 μg pCAGGS-HA-gB, pCAGGS-HA-gD, pCAGGS-HA-gH, pCAGGS-HA-gL, or control plasmids in 12-well plates for 24 h and then analyzed for the expression of NRP1 via Western blotting. (B) HEK293T cells and (D) RK13 cells were transfected with p-Flag-NRP1 with increasing amounts of pCAGGS-HA-gB or control. Western blots at 24 h posttransfection are shown. (C) HEK293T cells and (E) RK13 cells were cotransfected with 0.5 μg p-Flag-NRP1 and 2 μg pCAGGS-HA-gB or control and treated with MG132 (1 μM) or CQ (50, 100 μM). Western blotting was performed at 24 h posttransfection. (F) Western blot analysis of endogenous NRP1 in SH-SY5Y cells infected with PRV (MOI of 0.1), followed by treatment with CQ (100 μM). Twenty-four hours postinfection, the cells were subjected to Western blotting. All experiments were performed three times, and a representative result is shown. NRP1 degradation was quantified by densitometry scanning of Western blot images from three independent experiments. Band intensity ratio was shown, and band intensity ratio of control was set as 1. *, $P < 0.05$, **, $P < 0.01$.

FCS deficiency in gB significantly attenuated PRV virulence *in vivo* in mice. Furin has been reported to play an important role in viral pathogenesis in some viruses, including influenza virus and coronavirus (18, 19). In these viruses, the FCS can be efficiently cleaved by furin, which further affects viral infectivity, pathogenesis, transmission, and host range. Little is known about furin in PRV pathogenesis; therefore, we evaluated whether FCS in PRV gB also served as a PRV virulence factor. Mice were challenged with PRV gB-WT, PRV gB-Δ500R, PRV gB-Δ500-501RA, and PRV gB-Δfurin at the same dose. Four out of five mice survived PRV gB-Δfurin challenge, and three out of five mice survived PRV gB-Δ500-501RA challenge. These results indicated that the virulence of FCS-modified PRV was profoundly attenuated compared with wild-type PRV (Fig. 9A). We further detected the viral loads in tissues of the spleen, lung, kidney, and brain of the indicated challenged groups and found that viral copy numbers in PRV gB-Δ500-501RA- and PRV gB-Δfurin-infected mice were significantly lower than those in the PRV wild-type group (Fig. 9B). Finally, we further evaluated lung histopathological changes via histopathological examination (hematoxylin and eosin [H&E] staining), and the results indicated that the wild-type PRV and PRV gB-Δ500R groups developed severe microscopic lesions in the lung (Fig. 9C). In contrast, live mice in the PRV gB-Δ500-501RA and PRV gB-Δfurin challenge groups exhibited fewer histopathological changes in the lungs (Fig. 9C). Overall, furin may play an important role in PRV pathogenesis *in vivo*.

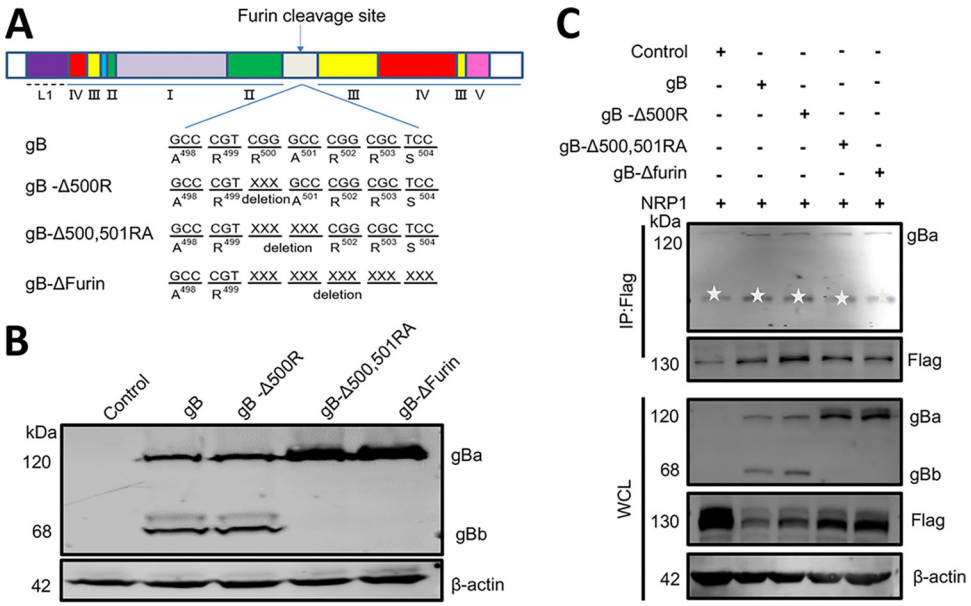

FIG 7 gB promotes the NRP1 degradation in a furin cleavage-dependent manner. (A) Schematic showing the deletion of the FCS from PRV gB. (B) To investigate whether gB interacts with NRP1, the plasmids pCAGGS-HA-gB-Δ500R, pCAGGS-HA-gB-Δ500-501RA, and pCAGGS-HA-gB-Δfurin were constructed. HEK293T cells were transfected with 1 μg gB, gB-Δ500R, gB-Δ500-501RA, gB-Δfurin, or control plasmids in 12-well plates, and 24 h later, the cells were analyzed via Western blotting. (C) HEK293T cells were cotransfected with 1.5 μg pCAGGS-HA-gB, pCAGGS-HA-gB-Δ500R, pCAGGS-HA-gB-Δ500-501RA, or pCAGGS-HA-gB-Δfurin and with 1.5 μg p-Flag-NRP1 or control plasmids in 6-well plates. Twenty-four hours later, the cells were subjected to IP with an antibody against Flag, followed by immunoblotting (IB) analysis for the complex with the indicated antibody. Star labeled band indicated as heavy chain of antibodies.

DISCUSSION

NRP1 is a host factor for SARS-CoV-2 cell entry and infectivity (25, 26). NRP1 is highly expressed in the respiratory system and olfactory epithelium and is also expressed in the central nervous system (CNS). In SARS-CoV-2 infection, NRP1 may play a role in viral-associated neurological symptoms (38, 39). In our study, we demonstrated that NRP1 was ubiquitously expressed in all tested organs in mice and pigs (data not shown). PRV is known to be a neurotropic virus (40–43). However, whether NRP1 contributes to PRV neurotropism and induces neurological symptoms was unclear. This may have been confirmed in conditional NRP1-knockout mice due to the lethality of the NRP1-knockout animals (44).

PRV virulence is determined by several viral pathogenicity-related genes (45–47). In previous reports, gB was found to be an essential gene for PRV replication (48, 49). However, no solid evidence to support gB was a virulence-related gene. In the current study, we demonstrated the virulence of PRV with gB FCS knockout was significantly attenuated in mice. This result demonstrated that the FCS in PRV plays an important role in PRV pathogenesis. This situation was similar to that of SARS-CoV-2, in which loss of the FCS attenuates its pathogenesis and transmission (50, 51). The loss of the FCS of SARS-CoV-2 may have a distinct effect on viral replication: Δfurin SARS-CoV-2 replicated faster in Vero E6 cells but replicated less efficiently in the human respiratory cell line Calu-3 (50). Interestingly, Δfurin PRV had the same replication kinetics and plaque size *in vitro* as the parental virus in the tested cells. We speculated that the FCS influenced PRV pathogenesis *in vivo* potentially due to its replicative activity *in vivo*. We found that the viral load of Δfurin PRV was significantly lower than that of the parental PRV, which is consistent with the H&E staining results. One limitation of this study is that we lacked a model to connect NRP1 and PRV pathogenesis *in vivo*. We recognize that NRP1 knockout mice may provide a direct connection between NRP1 and PRV pathogenesis. However, NRP1 is expressed in many cell types, including neurons and

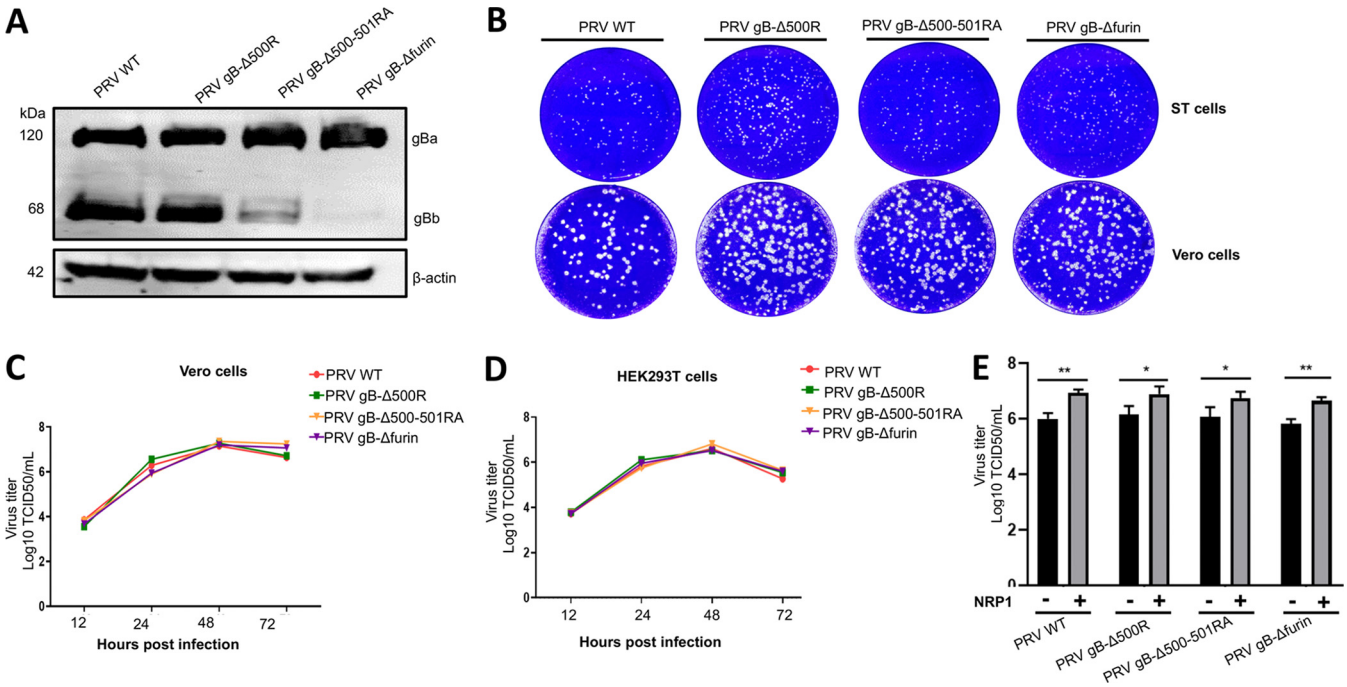

FIG 8 NRP1 promoted PRV replication through a CendR-independent pathway. (A) Vero cells were infected with PRV gB-WT, PRV gB-Δ500R, PRV gB-Δ500-501RA, or PRV gB-Δfurin (MOI of 0.1) and then collected at 24 h to detect the expression of gB. (B) Plaque morphology of PRV gB-WT, PRV gB-Δ500R, PRV gB-Δ500-501RA, and PRV gB-Δfurin in Vero and ST cells. ST and Vero cells were seeded in 6-well plates and infected with serial dilutions of PRV or PRV-gB mutant supernatants for 2 h at 37°C. The cells were then washed with PBS, overlaid with a mixture of 2% methyl cellulose and 2× DMEM containing 2% FBS, and incubated for 48 to 72 h. The plaques were counted. (C) Growth properties of the indicated viruses in Vero and (D) HEK293T cells. Cells cultured in 12-well plates were incubated with PRV or PRV-gB mutant at an MOI of 0.01 at 12-, 24-, 48-, and 72 hpi. Virus titers were determined using the 50% tissue culture infective dose (TCID50) method. (E) Vero cells were transfected with 1 μg control or p-Flag-NRP1 plasmid in 12-well plates for 24 h and then infected with PRV gB-WT, PRV gB-Δ500R, PRV gB-Δ500-501RA, or PRV gB-Δfurin at an MOI of 0.01. The virus titer was measured using a TCID50 assay at 24-hpi. All data are shown as the mean ± SD. **, $P < 0.01$; *, $P < 0.05$; Student's *t* test.

blood vessels, and NRP1 knockout in mice is embryonically lethal, with the mice having both neural and vascular defects (44). Furthermore, the attenuation observed after knockout of furin cleavage sites in PRV may be due to other unknown reasons, similar to knockout of furin cleavage sites in SARS-CoV-2 (50) and influenza virus (52), which also attenuated infection in tested animals.

In a recent study, the glycosylation of gB was shown to affect gB processing by furin cleavage and subsequently alter gB surface localization and fusogenicity (14). We also tested whether FCS knockout would influence gB-mediated fusogenicity and gB surface localization (data not shown). However, in our study, we found that the Δfurin construct did not exhibit altered gB fusogenicity or surface localization, as reported (14). This difference may be due to gB surface localization, and fusogenicity was indeed affected by glycosylation rather than furin cleavage. Furthermore, in the current study, we used a PRV variant, the PRV HeN1 strain (GenBank Accession No. KP098534), which is now epidemic in China (53). This strain exhibits marked sequence divergence compared with the sequence of European and American strains or Chinese strains isolated before 2000 (classic strains) (54). Whether the differences in gB between PRV variants and classic strains result in distinct results will be investigated in the future.

For most viruses, the interaction with NRP1 is CendR motif dependent (17). However, in our study, we demonstrated that the Δfurin gB construct retained the ability to interact with NRP1. However, we found gB weak interacted with NRP1. In this study, we found gBa could be IP-ed with NRP1 rather than gBb. Furthermore, we found most of gBa were cleaved by furin in cell lysate, this may be the reason that low level of gBa were detected in IP assay. Furthermore, gD and gH, which lack the CendR motif, also interacted with NRP1. This finding demonstrated that the interaction of PRV with NRP1 was independent of the CendR motif, which is distinct from other viruses. The

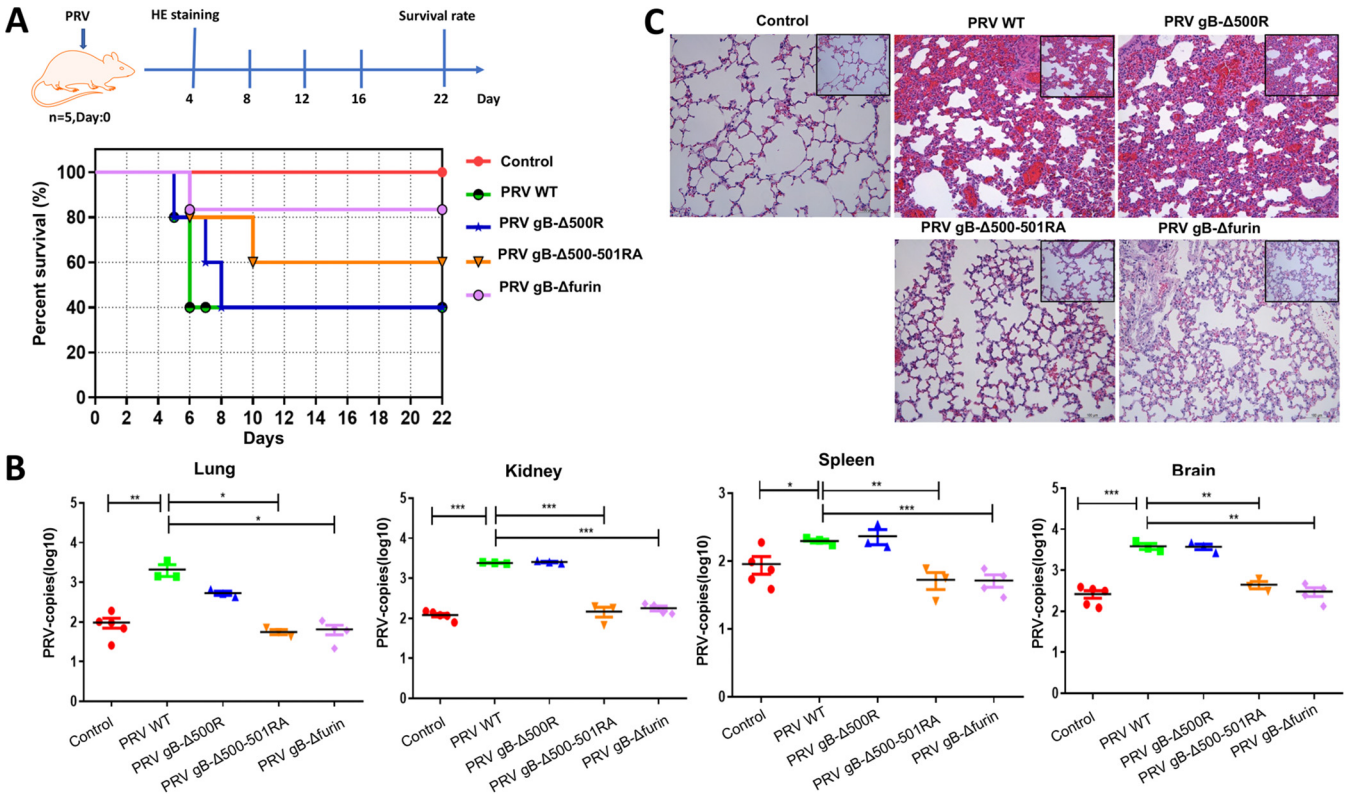

FIG 9 The PRV HeN1-gB mutant exhibits lower pathogenicity in mice than wild-type PRV. (A) Experimental strategy for PRV gB-WT, PRV gB-Δ500R, PRV gB-Δ500-501RA, or PRV gB-Δfurin challenge in mice. The survival rate was monitored daily for 15 days ($n = 5$ per group). (B) The viral load in the spleen, lung, kidney, and brain tissues of mice was determined using qRT–PCR. (C) At 15 days postchallenge, the remaining mice were euthanized, and microlesions in the lung tissues were examined via H&E staining (magnification = 100×). All data are shown as the mean ± SD, (***, $P < 0.001$; *, $P < 0.05$; **, $P < 0.01$).

detailed mechanism of this interaction and involved domains needs to be further explored.

NRP1 has been reported to be degraded by specific host factors or under conditions metabolic stress, and its degradation may occur via autophagy (55, 56). Viruses degraded host entry factors, especially its receptors may be common. Such as HSV-1 downregulated its receptor nectin-1 after virus infection (57, 58). And downregulated viral receptors may be the mechanism of superinfection resistance for some viruses (59). Our report is the first to show that viral-encoded proteins can promote NRP1 degradation, and this degradation is dependent on furin cleavage. Several cellular proteins are also degraded in a furin cleavage-dependent manner; however, the detailed mechanism is unclear (60, 61). There are many potential explanations, one simple explanation being that gB processed by furin targets NRP1 to lysosomal compartments, where NRP1 is degraded by resident proteases. This is a very interesting observation, and whether other viruses can degrade NRP1 and whether this degradation contributes to PRV neurological symptoms are unclear. All of these questions need further exploration.

Overall, our findings showed that NRP1 promotes PRV attachment and cell-to-cell fusion. Additionally, gB promotes NRP1 degradation via a lysosome-dependent pathway, and this process is dependent on furin. Finally, we demonstrated that gB FCS is a determinant of PRV virulence.

MATERIALS AND METHODS

Cells, viruses, antibodies, and plasmids. Rabbit kidney cells (RK13, ATCC CCL-37), human embryonic kidney cells (HEK293T, ATCC CRL-11268), African green monkey kidney cells (Vero, ATCC CCL-81; Vero-E6, ATCC CRL-1586), and swine testis cells (ST, ATCC CRL-1746) were maintained in Dulbecco's modified Eagle's medium (DMEM) (Gibco, USA) containing 10% fetal bovine serum (FBS, Excell, FND500). Human colon carcinoma cells (LoVo, ATCC CCL-229) and human neuroblastoma cell lines (SH-SY5Y, CRL-2266) were grown in RPMI 1640 medium with 10% FBS. A human neuroblastoma cell line (SK-N-SH) (Procell CL-0214)

was purchased from Procell (Wuhan, China) and maintained in SK-N-SH medium (Procell CM-0214). CHO cells were stored in our laboratory. These cells were maintained in 5% CO_2 at 37°C.

The PRV strain HeN1 (GenBank Accession No. KP098534) was stored at −80°C in our laboratory. The PRV strain HeN1-GFP was maintained as described in our previous report (32). The PRV strain rPRVTJ-NLuc was kindly provided by Yuan Sun at our institute (34).

Anti-β-actin antibody (Proteintech, China), anti-NRP1 antibody (mouse; Proteintech, China), anti-NRP1 antibody (rabbit; CST, USA), anti-PVRL1 antibody (Nectin-1) (Proteintech, China), anti-Flag antibody (Sigma, USA), anti-HA antibody (Sigma, USA), anti-mouse IgG-FITC antibody (Sigma, USA), and Alexa Fluor 488-conjugated and Alexa Fluor 568-conjugated secondary antibodies for immunostaining were purchased from Invitrogen. The mouse anti-PRV gB monoclonal antibody (1E7) was kindly provided by Zhi-Jun Tian at our institute. The epitope identified by the gB antibody was 81-SAEESLE-87 of the gB protein; therefore, we can see two bands for gB. The large band is the full-length gBa, and the small band is the cleavage fragment of gBb.

The pCAGGS-HA-gB, pCAGGS-HA-gD, pCAGGS-HA-gH, pCAGGS-HA-gL, pCDNA3.1-Flag, pCAGGS-HA, and pDC315-EGFP plasmids were stored in our laboratory and have been described in our previous studies (62, 63). The pCMV3-C-Flag-Nectin1 plasmid and pCDNA3.1-Flag-NRP1 plasmid were purchased from Sino Biological (Beijing, China). pCMV-Red-NRP1 was constructed by our laboratory.

Quantitative real-time polymerase chain reaction (qRT-PCR). Viral DNA was extracted with the TIANamp Genomic DNA Kit (Tiangen, China) according to the manufacturer's instructions. This method was used to quantify the copy number of the gB gene of PRV, as described in our previous report (37). The specific primer sequences for the gB genes are shown in Table S1.

Semiquantitative PCR detection of NRP1 in tissues. The mRNA levels of NRP1 and β-actin were determined by nested semiquantitative PCR. Total RNA was extracted from tissue using a Total RNA Kit I (Tiangen, China) and reversed transcribed to generate cDNA by Reverse Transcriptase M-MLV (TaKaRa, China) according to the manufacturer's protocol. Then, nested semiquantitative PCR was performed, and β-actin was used as an internal reference. The specific primer sequences for the target genes are shown in Table S2.

NRP1 siRNA knockdown. A small interference RNA (siRNA) assay was performed to confirm the target gene of NRP1 with siRNA synthesized by GenePharma (Shanghai, China). Briefly, cells were seeded in 12-well plates (60% to 80% confluence) and transfected with siNRP1 or negative control (NC) using Lipofectamine RNAiMAX (Invitrogen) at a final concentration of 60 nM following the manufacturer's instructions. At 48-h posttransfection, the protein levels were confirmed by Western blotting. The siRNA sequences are shown in Table S3.

PRV attachment assay. CHO and HEK293T cells were seeded in 12-well plates. When the cells reached 70% to 80% confluence, 1 μg of the control or p-Flag-NRP1 plasmid was transfected. Overexpression plasmids were transfected using jetPRIME (Polyplus Transfection, France) according to the manufacturer's instructions. At 24-h posttransfection, cells were infected with PRV-HeN1 (MOI = 1) and maintained at 4°C. Two hours later, the cells were washed three times with cold PBS, and DNA was extracted with a TIANamp Genomic DNA Kit (Tiangen, China) and quantified by qPCR.

PRV entry assay. Virus entry was evaluated by infection with rPRVTJ-NLuc, which expresses NanoLuc luciferase. CHO cells were transfected with plasmids expressing p-Flag-NRP1, p-Nectin-1, or control DNA. After 24 h, the transfected cells were infected with rPRVTJ-NLuc (1∼4 × 10^6 PFU/well). The cells were maintained in 5% CO_2 at 37°C. Six hours after inoculation, the supernatants were removed, and the cells were washed three times with PBS. Cells were lysed with cell culture lysis buffer (Promega, USA). Cell lysates were assayed with the Nano-Glo Luciferase Assay System (Promega, USA), and luciferase activity was determined.

Cell-to-cell fusion assay. HEK293T or RK13 cells were seeded in 24-well plates. When they reached 80% to 90% confluence, the cells were cotransfected with 500 ng of p-Flag-NRP1; 200 ng of EGFP expression plasmid (pDC315-EGFP); and pCAGGS-HA-gB, pCAGGS-HA-gD, pCAGGS-HA-gL, and pCAGGS-HA-gH or control plasmids according to the manufacturer's instructions. Twenty-four hours after transfection, the cells were observed by fluorescence microscopy. Fusion activity was evaluated based on the relative EGFP furin area, which was quantified by ImageJ software. The furin activity of the control group was set as 100%.

Cell-to-cell membrane fusion was also detected using a luciferase assay, as described in our previous report (64). Briefly, when HEK293T cells grew to 90% confluence in a 6-well plate, the cells in one well were transfected with 0.5 μg of pGL5-Luc (Promega, USA), and those in other wells were cotransfected with 2 μg of pBind-Id (Promega, USA) and 2 μg of PACT-Myod (Promega, USA). Twelve hours later, the transfected pGL5-Luc cells were mixed 1:1 with cotransfected pBind-ID and PACT-Myod cells or empty cells. Twelve hours later, p-Flag-NRP1 and pCAGGS-HA-gB, pCAGGS-HA-gD, pCAGGS-HA-gL, pCAGGS-HA-gH, or control plasmids were cotransfected. The luciferase activity was measured 48 h later with the Luciferase Assay System (Promega, USA). The furin activity of the control group was set to 100%.

Coimmunoprecipitation assay. HEK293T cells grown to approximately 70% to 80% confluence in 6-well plates were cotransfected with p-Flag-NRP1 and pCAGGS-HA-gB, pCAGGS-HA-gD, pCAGGS-HA-gL, pCAGGS-HA-gH, or control plasmids (3 μg/well). At 24-h posttransfection, the cells were lysed with RIPA lysis buffer (Beyotime Biotechnology, China) containing PMSF (Beyotime Biotechnology, China) and a complete protease inhibitor cocktail (Sigma–Aldrich, USA) for 1 h on ice. The cell lysates were centrifuged at 12,000 × g for 10 min, and 100 μL of supernatant was taken as the input sample. The rest of the supernatant was incubated with 20 μL of FLAG M2 beads (Sigma, USA) at 4°C for 6 to 8 h. Subsequently, the beads were rinsed with PBS (pH =7.4) three times (20 min/time) at 4°C, and

precipitates were eluted in 60 μL of lysis buffer and 4$\times$ loading buffer (Solarbio, China) by boiling at 100°C for 8 to 10 min. The samples were detected by Western blotting.

For Western blotting, cells were washed twice with cold PBS and lysed in NP-40 buffer (Beyotime Biotechnology, China). The protein concentration was measured using a BCA protein assay kit (Solarbio, China). Cell lysates were boiled in 4$\times$ loading buffer for 10 min, and equal amounts of samples were then subjected to SDS–PAGE. The separated proteins were transferred to PVDF membranes (Millipore, USA). The membranes were blocked with 5% nonfat milk in PBS for 1 h and incubated with an antibody overnight at 4°C, followed by washing and incubation with the appropriate secondary antibody for 1 h at room temperature. Detection was performed with fluorescent secondary antibodies, and visualization was carried out with the Odyssey CLx imaging system.

BiFC assay. The plasmids pVC-gB, pVC-gD, pVC-gH, pVC-gL, and pVN-NRP1 were constructed via homologous recombination. The specific primer sequences are shown in Table S4. In the present study, the BiFC system was used to visualize the interaction between gB, gD, gH, and gL and NRP1 in HEK293T cells. Briefly, the open reading frame (ORF) sequences of gB, gD, gH, gL, and NRP1 were amplified and inserted into the plasmids pVC and pVN which contain the Venus C-terminal or N-terminal fragment, respectively. The final plasmids were named pVC-gB, pVC-gD, pVC-gH, pVC-gL, and pVN-NRP1. HEK293T cells were cotransfected with pVN-NRP1 and with pVC-gB, pVC-gD, pVC-gH, or pVC-gL. pVC and pVN only contained the ORF of VC or VN were uses as a control in this study. The fluorescence signals were observed via confocal microscopy.

gB promoted decreases in exogenous and endogenous NRP1. To assess the exogenous degradation of NRP1, HEK293T and RK13 cells were seeded in 12-well plates. When the cells reached 90% confluence, Flag-NRP1 plasmid (0.5 μg) and gB plasmid at different doses were used o transfect the cells. The cells were collected 24 h later, and the expression level of NRP1 was analyzed by Western blotting. There are two major pathways of intracellular protein degradation: the ubiquitin–proteasome-dependent pathway and the lysosome-dependent pathway. To determine whether these two pathways are involved in gB-mediated NRP1 degradation, MG132 (a ubiquitin–proteasome inhibitor, Sigma, 1 μM) and CQ (a lysosome pathway inhibitor, Sigma, 50 and 100 μM) were added to HEK293T and RK13 cells coexpressing gB (2 μg) and NRP1 (0.5 μg).

To test the endogenous degradation of NRP1, SH-SY5Y cells grown to approximately 90% confluence in 12-well plates were pretreated with CQ (100 μM) for 2 h and infected with PRV at an MOI of 0.1. After 24 h, the cells were harvested, and the expression level of endogenous NRP1 was detected by Western blotting.

Construction of gB mutants. The gB-CendR mutation plasmids gB-Δ500R, gB-Δ500-501RA, and gB-Δfurin were constructed by site-directed mutagenesis. The plasmid construction process was as follows: the 100-μL reaction mixture contained 1 μg of pCAGGS-HA-gB, 50 μL of 2 $\times$ KOD buffer, 8 μL of dNTP, 2 μL of forward primer (10 μM), 2 μL of reverse primer (10 μM), 2 μL of KOD enzyme (Toyobo, Japan), and 35 μL of H_2O. The PCR procedure was as follows: initial denaturation at 95°C for 5 min and 21 cycles of denaturation at 94°C for 30 s, annealing at 56°C for 30 s and amplification at 72°C for 5 min. Then, 200 μL of anhydrous ethanol was added to the sample, which was incubated for 10 min at room temperature. Finally, the samples were centrifuged at 12,000 $\times$ *g* for 10 min, and DpnI (Thermo Fisher Scientific, USA) was added for digestion. The digestion reaction was as follows: the 20-μL reaction mixture contained 17 μL of H_2O, 2 μL of 10 $\times$ FastDigest Buffer, and 1 μL of DpnI. All clones were verified by DNA sequencing. Primers are shown in Table S1.

Δfurin virus construction by the CRISPR system. PRV FCS knockout viruses were generated as previously described (37, 45, 46, 48). sgRNAs targeting the gB gene were designed using the CRISPR Design Tool (65). ssDNA used for precision recombination was synthesized by Tsingke Biotechnology. The sgRNA sequences and the primers used for PCR identification are shown in Table S2. Briefly, HEK293T cells were plated into a 6-well plate, and 12 h later, 3 μg of the PRV HeN1 genome, 2 μg of the CRISPR/Cas9 plasmid, and 3 μg of the indicated ssDNA were cotransfected. After CPE was observed, the cell cultures were collected. PRV gB-Δ500R, PRV gB-Δ500-501RA, and PRV gB-Δfurin were purified by plaque purification. PRV FCS knockout virus was confirmed by DNA sequencing.

Viral growth curves and plaque assays. Vero and HEK293T cells cultured in 12-well plates were incubated with PRV gB-WT, PRV gB-Δ500R, PRV gB-Δ500-501RA, and PRV gB-Δfurin at an MOI of 0.01 for 2 h at 37°C. Then, the inoculum was removed, and DMEM supplemented with 2% FBS was added to each well. At 12-, 24-, 48-, and 72-hpi, the cells and supernatants were harvested and stored at 80°C. The virus titers were determined using the 50% tissue culture infective dose (TCID50) method.

For plaque assays, ST and Vero cells were seeded in 6-well plates and infected with serial dilutions of PRV or PRV-gB mutant supernatants for 2 h at 37°C. The cells were then washed with PBS, overlaid with a mixture of 2% methyl cellulose and 2$\times$ DMEM containing 2% FBS, and incubated for 48 to 72 h at 37°C in 5% CO_2. The cells were stained with saturated crystal violet for 30 min at room temperature before the plaques were counted.

Challenge experiments with mice. Twenty-five 6-week-old female specific-pathogen-free mice were randomly divided into five groups. The mice in groups 1 to 4 were inoculated intramuscularly with 10^4 TCID50 of PRV gB-WT, PRV gB-Δ500R, PRV gB-Δ500-501RA, and PRV gB-Δfurin, respectively. The mice in group 5 were inoculated intramuscularly with PBS and used as negative controls. The mice were observed daily.

H&E staining and viral load detection. At 14 days post-challenge (dpc), the remaining mice were euthanized, and tissue samples were collected and subjected to histopathological analysis after H&E staining. Viruses were detected using qPCR. For viral load detection, total viral DNA was extracted from 25-mg tissue samples using a TIANamp Virus DNA/RNA Kit (Tiangen, China) according to the manufacturer's instructions. The control group consisted of five surviving mice; the PRV gB-WT group consisted

of three dead mice; the PRV gB-Δ500R group consisted of three dead mice; the PRV gB-Δ500-501RA group consisted of three surviving mice; and the PRV gB-Δfurin group consisted of four surviving mice. The probe and primers are listed in Table S1.

Ethics statement. All animal experiments were conducted in accordance with the Guide for the Care and Use of Laboratory Animals of the Ministry of Science and Technology of the People's Republic of China. Animal experiments (approval number: 211116-03; approval number: 211202-01) were carried out in animal biosafety level 2 facilities under the supervision of the Committee on the Ethics of Animal Experiments of the Harbin Veterinary Research Institute of the Chinese Academy of Agricultural Sciences (CAAS).

Statistical analysis. Statistical analysis was performed using GraphPad Prism 8.0 software, and Student's *t* test was used with at least three independent replicates. Differences with a P value <0.05 for each test were considered statistically significant.

SUPPLEMENTAL MATERIAL

Supplemental material is available online only.

SUPPLEMENTAL FILE 1, PDF file, 0.2 MB.

ACKNOWLEDGMENTS

This research was funded by the National Natural Science Foundation of China 32202776 (M.-H.W.), and the State Key Laboratory of Veterinary Biotechnology Foundation from Harbin Veterinary Research Institute of the Chinese Academy of Agricultural Sciences (SKLVBF202211).

We thank Yuan Sun of Harbin Veterinary Research Institute of the Chinese Academy of Agricultural Sciences for providing the reporter virus.

REFERENCES

1. Davison A, Eberle R, Ehlers B, Hayward G, McGeoch D, Minson A, Pellett P, Roizman B, Studdert M, Thiry E. 2009. The order Herpesvirales. Arch Virol 154:171–177. https://doi.org/10.1007/s00705-008-0278-4.
2. Mettenleiter TC. 1991. Molecular biology of pseudorabies (Aujeszky's disease) virus. Comp Immunol Microbiol Infect Dis 14:151–163. https://doi.org/10.1016/0147-9571(91)90128-Z.
3. Mettenleiter T. 2000. Aujeszky's disease (pseudorabies) virus: the virus and molecular pathogenesis–state of the art, June 1999. Vet Res 31:99–115. https://doi.org/10.1051/vetres:2000110.
4. Mettenleiter TC. 2020. Aujeszky's disease and the development of the marker/DIVA vaccination concept. Pathogens 9:563. https://doi.org/10.3390/pathogens9070563.
5. Wong G, Lu J, Zhang W, Gao GF. 2019. Pseudorabies virus: a neglected zoonotic pathogen in humans? Emerg Microbes Infect 8:150–154. https://doi.org/10.1080/22221751.2018.1563459.
6. Ai JW, Weng SS, Cheng Q, Cui P, Li YJ, Wu HL, Zhu YM, Xu B, Zhang WH. 2018. Human endophthalmitis caused by pseudorabies virus infection, China, 2017. Emerg Infect Dis 24:1087–1090. https://doi.org/10.3201/eid2406.171612.
7. Liu Q, Wang X, Xie C, Ding S, Yang H, Guo S, Li J, Qin L, Ban F, Wang D, Wang C, Feng L, Ma H, Wu B, Zhang L, Dong C, Xing L, Zhang J, Chen H, Yan R, Wang X, Li W. 2021. A novel human acute encephalitis caused by pseudorabies virus variant strain. Clin Infect Dis 73:e3690–e3700. https://doi.org/10.1093/cid/ciaa987.
8. Yang X, Guan H, Li C, Li Y, Wang S, Zhao X, Zhao Y, Liu Y. 2019. Characteristics of human encephalitis caused by pseudorabies virus: a case series study. Int J Infect Dis 87:92–99. https://doi.org/10.1016/j.ijid.2019.08.007.
9. Rauh I, Mettenleiter T. 1991. Pseudorabies virus glycoproteins gII and gp50 are essential for virus penetration. J Virol 65:5348–5356. https://doi.org/10.1128/JVI.65.10.5348-5356.1991.
10. Vallbracht M, Backovic M, Klupp BG, Rey FA, Mettenleiter TC. 2019. Common characteristics and unique features: a comparison of the fusion machinery of the alphaherpesviruses Pseudorabies virus and Herpes simplex virus. Adv Virus Res 104:225–281. https://doi.org/10.1016/bs.aivir.2019.05.007.
11. Peeters B, de Wind N, Broer R, Gielkens A, Moormann R. 1992. Glycoprotein H of pseudorabies virus is essential for entry and cell-to-cell spread of the virus. J Virol 66:3888–3892. https://doi.org/10.1128/JVI.66.6.3888-3892.1992.
12. Spear PG, Eisenberg RJ, Cohen GH. 2000. Three classes of cell surface receptors for alphaherpesvirus entry. Virology 275:1–8. https://doi.org/10.1006/viro.2000.0529.
13. Vallbracht M, Brun D, Tassinari M, Vaney MC, Pehau-Arnaudet G, Guardado-Calvo P, Haouz A, Klupp BG, Mettenleiter TC, Rey FA, Backovic M. 2018. Structure-function dissection of pseudorabies virus glycoprotein B fusion loops. J Virol 92. https://doi.org/10.1128/JVI.01203-17.
14. Vallbracht M, Klupp BG, Mettenleiter TC. 2021. Influence of N-glycosylation on expression and function of pseudorabies virus glycoprotein gB. Pathogens 10:61. https://doi.org/10.3390/pathogens10010061.
15. Okazaki K. 2007. Proteolytic cleavage of glycoprotein B is dispensable for in vitro replication, but required for syncytium formation of pseudorabies virus. J Gen Virol 88:1859–1865. https://doi.org/10.1099/vir.0.82610-0.
16. Hampl H, Ben-Porat T, Ehrlicher L, Habermehl K, Kaplan A. 1984. Characterization of the envelope proteins of pseudorabies virus. J Virol 52:583–590. https://doi.org/10.1128/JVI.52.2.583-590.1984.
17. Balistreri G, Yamauchi Y, Teesalu T. 2021. A widespread viral entry mechanism: the C-end rule motif-neuropilin receptor interaction. Proc Natl Acad Sci U S A 118. https://doi.org/10.1073/pnas.2112457118.
18. Hossain MG, Tang YD, Akter S, Zheng C. 2022. Roles of the polybasic furin cleavage site of spike protein in SARS-CoV-2 replication, pathogenesis, and host immune responses and vaccination. J Med Virol 94:1815–1820. https://doi.org/10.1002/jmv.27539.
19. Whittaker GR. 2021. SARS-CoV-2 spike and its adaptable furin cleavage site. Lancet Microbe 2:e488–e489. https://doi.org/10.1016/S2666-5247(21)00174-9.
20. Shang J, Wan Y, Luo C, Ye G, Geng Q, Auerbach A, Li F. 2020. Cell entry mechanisms of SARS-CoV-2. Proc Natl Acad Sci U S A 117:11727–11734. https://doi.org/10.1073/pnas.2003138117.
21. Braun E, Sauter D. 2019. Furin-mediated protein processing in infectious diseases and cancer. Clin Transl Immunology 8:e1073. https://doi.org/10.1002/cti2.1073.
22. Pang HB, Braun GB, Friman T, Aza-Blanc P, Ruidiaz ME, Sugahara KN, Teesalu T, Ruoslahti E. 2014. An endocytosis pathway initiated through neuropilin-1 and regulated by nutrient availability. Nat Commun 5:4904. https://doi.org/10.1038/ncomms5904.
23. Teesalu T, Sugahara KN, Kotamraju VR, Ruoslahti E. 2009. C-end rule peptides mediate neuropilin-1-dependent cell, vascular, and tissue penetration. Proc Natl Acad Sci U S A 106:16157–16162. https://doi.org/10.1073/pnas.0908201106.
24. Wang H, Zhang H, Zhang J, Li Y, Zhao B, Feng G, Du Y, Xiong D, Zhong Q, Liu W, Du H, Li M, Huang W, Tsao S, Hutt-Fletcher L, Zeng Y, Kieff E, Zeng

M. 2015. Neuropilin 1 is an entry factor that promotes EBV infection of nasopharyngeal epithelial cells. Nat Commun 6:6240. https://doi.org/10.1038/ncomms7240.
25. Cantuti-Castelvetri L, Ojha R, Pedro L, Djannatian M, Franz J, Kuivanen S, van der Meer F, Kallio K, Kaya T, Anastasina M, Smura T, Levanov L, Szirovicza L, Tobi A, Kallio-Kokko H, Österlund P, Joensuu M, Meunier F, Butcher S, Winkler M, Mollenhauer B, Helenius A, Gokce O, Teesalu T, Hepojoki J, Vapalahti O, Stadelmann C, Balistreri G, Simons M. 2020. Neuropilin-1 facilitates SARS-CoV-2 cell entry and infectivity. Science 370:856–860. https://doi.org/10.1126/science.abd2985.
26. Daly J, Simonetti B, Klein K, Chen K, Williamson M, Antón-Plágaro C, Shoemark D, Simón-Gracia L, Bauer M, Hollandi R, Greber U, Horvath P, Sessions R, Helenius A, Hiscox J, Teesalu T, Matthews D, Davidson A, Collins B, Cullen P, Yamauchi Y. 2020. Neuropilin-1 is a host factor for SARS-CoV-2 infection. Science 370:861–865. https://doi.org/10.1126/science.abd3072.
27. Mayi BS, Leibowitz JA, Woods AT, Ammon KA, Liu AE, Raja A. 2021. The role of Neuropilin-1 in COVID-19. PLoS Pathog 17:e1009153. https://doi.org/10.1371/journal.ppat.1009153.
28. Ghez D, Lepelletier Y, Lambert S, Fourneau JM, Blot V, Janvier S, Arnulf B, van Endert PM, Heveker N, Pique C, Hermine O. 2006. Neuropilin-1 is involved in human T-cell lymphotropic virus type 1 entry. J Virol 80:6844–6854. https://doi.org/10.1128/JVI.02719-05.
29. Lambert S, Bouttier M, Vassy R, Seigneuret M, Petrow-Sadowski C, Janvier S, Heveker N, Ruscetti FW, Perret G, Jones KS, Pique C. 2009. HTLV-1 uses HSPG and neuropilin-1 for entry by molecular mimicry of VEGF165. Blood 113:5176–5185. https://doi.org/10.1182/blood-2008-04-150342.
30. Lane RK, Guo H, Fisher AD, Diep J, Lai Z, Chen Y, Upton JW, Carette J, Mocarski ES, Kaiser WJ. 2020. Necroptosis-based CRISPR knockout screen reveals Neuropilin-1 as a critical host factor for early stages of murine cytomegalovirus infection. Proc Natl Acad Sci U S A 117:20109–20116. https://doi.org/10.1073/pnas.1921315117.
31. Wang S, Zhao L, Zhang X, Zhang J, Shang H, Liang G. 2022. Neuropilin-1, a myeloid cell-specific protein, is an inhibitor of HIV-1 infectivity. Proc Natl Acad Sci U S A 119.
32. Tang YD, Liu JT, Fang QQ, Wang TY, Sun MX, An TQ, Tian ZJ, Cai XH. 2016. Recombinant pseudorabies virus (PRV) expressing firefly luciferase effectively screened for CRISPR/Cas9 single guide RNAs and antiviral compounds. Viruses 8:90. https://doi.org/10.3390/v8040090.
33. Geraghty R, Krummenacher C, Cohen G, Eisenberg R, Spear P. 1998. Entry of alphaherpesviruses mediated by poliovirus receptor-related protein 1 and poliovirus receptor. Science 280:1618–1620. https://doi.org/10.1126/science.280.5369.1618.
34. Wang Y, Wu H, Wang B, Qi H, Jin Z, Qiu HJ, Sun Y. 2020. A NanoLuc luciferase reporter pseudorabies virus for live imaging and quantification of viral infection. Front Vet Sci 7:566446. https://doi.org/10.3389/fvets.2020.566446.
35. Atanasiu D, Whitbeck J, Cairns T, Reilly B, Cohen G, Eisenberg R. 2007. Bimolecular complementation reveals that glycoproteins gB and gH/gL of herpes simplex virus interact with each other during cell fusion. Proc Natl Acad Sci U S A 104:18718–18723. https://doi.org/10.1073/pnas.0707452104.
36. Atanasiu D, Whitbeck J, de Leon M, Lou H, Hannah B, Cohen G, Eisenberg R. 2010. Bimolecular complementation defines functional regions of Herpes simplex virus gB that are involved with gH/gL as a necessary step leading to cell fusion. J Virol 84:3825–3834. https://doi.org/10.1128/JVI.02687-09.
37. Tang YD, Guo JC, Wang TY, Zhao K, Liu JT, Gao JC, Tian ZJ, An TQ, Cai XH. 2018. CRISPR/Cas9-mediated 2-sgRNA cleavage facilitates pseudorabies virus editing. FASEB J 32:4293–4301. https://doi.org/10.1096/fj.201701129R.
38. Davies J, Randeva HS, Chatha K, Hall M, Spandidos DA, Karteris E, Kyrou I. 2020. Neuropilin1 as a new potential SARSCoV2 infection mediator implicated in the neurologic features and central nervous system involvement of COVID19. Mol Med Rep 22:4221–4226. https://doi.org/10.3892/mmr.2020.11510.
39. Moutal A, Martin LF, Boinon L, Gomez K, Ran D, Zhou Y, Stratton HJ, Cai S, Luo S, Gonzalez KB, Perez-Miller S, Patwardhan A, Ibrahim MM, Khanna R. 2021. SARS-CoV-2 spike protein co-opts VEGF-A/neuropilin-1 receptor signaling to induce analgesia. Pain 162:243–252. https://doi.org/10.1097/j.pain.0000000000002097.
40. Card JP, Rinaman L, Schwaber JS, Miselis RR, Whealy ME, Robbins AK, Enquist LW. 1990. Neurotropic properties of pseudorabies virus: uptake and transneuronal passage in the rat central nervous system. J Neurosci 10:1974–1994. https://doi.org/10.1523/JNEUROSCI.10-06-01974.1990.
41. Laval K, Enquist LW. 2020. The neuropathic itch caused by pseudorabies virus. Pathogens 9:254. https://doi.org/10.3390/pathogens9040254.
42. Enquist LW. 2002. Exploiting circuit-specific spread of pseudorabies virus in the central nervous system: insights to pathogenesis and circuit tracers. J Infect Dis 186 Suppl 2:S209–14. https://doi.org/10.1086/344278.
43. Tirabassi RS, Townley RA, Eldridge MG, Enquist LW. 1998. Molecular mechanisms of neurotropic herpesvirus invasion and spread in the CNS. Neurosci Biobehav Rev 22:709–720. https://doi.org/10.1016/s0149-7634(98)00009-8.
44. Fernandez-Robredo P, Selvam S, Powner MB, Sim DA, Fruttiger M. 2017. Neuropilin 1 involvement in choroidal and retinal neovascularisation. PLoS One 12:e0169865. https://doi.org/10.1371/journal.pone.0169865.
45. Tang YD, Liu JT, Wang TY, Sun MX, Tian ZJ, Cai XH. 2017. Comparison of pathogenicity-related genes in the current pseudorabies virus outbreak in China. Sci Rep 7:7783. https://doi.org/10.1038/s41598-017-08269-3.
46. Tang YD, Liu JT, Wang TY, An TQ, Sun MX, Wang SJ, Fang QQ, Hou LL, Tian ZJ, Cai XH. 2016. Live attenuated pseudorabies virus developed using the CRISPR/Cas9 system. Virus Res 225:33–39. https://doi.org/10.1016/j.virusres.2016.09.004.
47. Delva JL, Nauwynck HJ, Mettenleiter TC, Favoreel HW. 2020. The attenuated pseudorabies virus vaccine strain Bartha K61: a brief review on the knowledge gathered during 60 years of research. Pathogens 9:897. https://doi.org/10.3390/pathogens9110897.
48. Wang T-Y, Sang G-J, Wang Q, Leng C-L, Tian Z-J, Peng J-M, Wang S-J, Sun M-X, Meng F-D, Zheng H, Cai X-H, Tang Y-D. 2022. Generation of premature termination codon (PTC)-harboring pseudorabies virus (PRV) via genetic code expansion technology. Viruses 14:572. https://doi.org/10.3390/v14030572.
49. Rauh I, Weiland F, Fehler F, Keil G, Mettenleiter T. 1991. Pseudorabies virus mutants lacking the essential glycoprotein gII can be complemented by glycoprotein gI of bovine herpesvirus 1. J Virol 65:621–631. https://doi.org/10.1128/JVI.65.2.621-631.1991.
50. Johnson BA, Xie X, Bailey AL, Kalveram B, Lokugamage KG, Muruato A, Zou J, Zhang X, Juelich T, Smith JK, Zhang L, Bopp N, Schindewolf C, Vu M, Vanderheiden A, Winkler ES, Swetnam D, Plante JA, Aguilar P, Plante KS, Popov V, Lee B, Weaver SC, Suthar MS, Routh AL, Ren P, Ku Z, An Z, Debbink K, Diamond MS, Shi PY, Freiberg AN, Menachery VD. 2021. Loss of furin cleavage site attenuates SARS-CoV-2 pathogenesis. Nature 591:293–299. https://doi.org/10.1038/s41586-021-03237-4.
51. Peacock TP, Goldhill DH, Zhou J, Baillon L, Frise R, Swann OC, Kugathasan R, Penn R, Brown JC, Sanchez-David RY, Braga L, Williamson MK, Hassard JA, Staller E, Hanley B, Osborn M, Giacca M, Davidson AD, Matthews DA, Barclay WS. 2021. The furin cleavage site in the SARS-CoV-2 spike protein is required for transmission in ferrets. Nat Microbiol 6:899–909. https://doi.org/10.1038/s41564-021-00908-w.
52. Rott R, Klenk H, Nagai Y, Tashiro M. 1995. Influenza viruses, cell enzymes, and pathogenicity. Am J Respir Crit Care Med 152:S16–9. https://doi.org/10.1164/ajrccm/152.4_Pt_2.S16.
53. An TQ, Peng JM, Tian ZJ, Zhao HY, Li N, Liu YM, Chen JZ, Leng CL, Sun Y, Chang D, Tong GZ. 2013. Pseudorabies virus variant in Bartha-K61-vaccinated pigs, China, 2012. Emerg Infect Dis 19:1749–1755. https://doi.org/10.3201/eid1911.130177.
54. Ye C, Zhang QZ, Tian ZJ, Zheng H, Zhao K, Liu F, Guo JC, Tong W, Jiang CG, Wang SJ, Shi M, Chang XB, Jiang YF, Peng JM, Zhou YJ, Tang YD, Sun MX, Cai XH, An TQ, Tong GZ. 2015. Genomic characterization of emergent pseudorabies virus in China reveals marked sequence divergence: evidence for the existence of two major genotypes. Virology 483:32–43. https://doi.org/10.1016/j.virol.2015.04.013.
55. Bae D, Lu S, Taglienti CA, Mercurio AM. 2008. Metabolic stress induces the lysosomal degradation of neuropilin-1 but not neuropilin-2. J Biol Chem 283:28074–28080. https://doi.org/10.1074/jbc.M804203200.
56. Okon IS, Coughlan KA, Zhang C, Moriasi C, Ding Y, Song P, Zhang W, Li G, Zou MH. 2014. Protein kinase LKB1 promotes RAB7-mediated neuropilin-1 degradation to inhibit angiogenesis. J Clin Invest 124:4590–4602. https://doi.org/10.1172/JCI75371.
57. Stiles K, Krummenacher C. 2010. Glycoprotein D actively induces rapid internalization of two nectin-1 isoforms during herpes simplex virus entry. Virology 399:109–119. https://doi.org/10.1016/j.virol.2009.12.034.
58. Stiles K, Milne R, Cohen G, Eisenberg R, Krummenacher C. 2008. The herpes simplex virus receptor nectin-1 is down-regulated after trans-interaction with glycoprotein D. Virology 373:98–111. https://doi.org/10.1016/j.virol.2007.11.012.
59. Nethe M, Berkhout B, van der Kuyl A. 2005. Retroviral superinfection resistance. Retrovirology 2:52. https://doi.org/10.1186/1742-4690-2-52.
60. Gagliardo B, Kubat N, Faye A, Jaouen M, Durel B, Deschemin JC, Canonne-Hergaux F, Sari MA, Vaulont S. 2009. Pro-hepcidin is unable to degrade

the iron exporter ferroportin unless maturated by a furin-dependent process. J Hepatol 50:394–401. https://doi.org/10.1016/j.jhep.2008.09.018.
61. Milner JM, Rowan AD, Elliott SF, Cawston TE. 2003. Inhibition of furin-like enzymes blocks interleukin-1alpha/oncostatin M-stimulated cartilage degradation. Arthritis Rheum 48:1057–1066. https://doi.org/10.1002/art.10873.
62. Tang Y, Na L, Zhu C, Shen N, Yang F, Fu X, Wang Y, Fu L, Wang J, Lin Y, Wang X, Wang X, Zhou J, Li C. 2014. Equine viperin restricts equine infectious anemia virus replication by inhibiting the production and/or release of viral Gag, Env, and receptor via distortion of the endoplasmic reticulum. J Virol 88:12296–12310. https://doi.org/10.1128/JVI.01379-14.
63. Wang Y, Liu T, Wang T, Tang Y, Wei P. 2020. Isobavachalcone inhibits Pseudorabies virus by impairing virus-induced cell-to-cell fusion. Virol J 17:39. https://doi.org/10.1186/s12985-020-01312-2.
64. Yang YL, Meng F, Qin P, Herrler G, Huang YW, Tang YD. 2020. Trypsin promotes porcine deltacoronavirus mediating cell-to-cell fusion in a cell type-dependent manner. Emerg Microbes Infect 9:457–468. https://doi.org/10.1080/22221751.2020.1730245.
65. Stemmer M, Thumberger T, Del Sol Keyer M, Wittbrodt J, Mateo JL. 2015. CCTop: an intuitive, flexible and reliable CRISPR/Cas9 target prediction tool. PLoS One 10:e0124633. https://doi.org/10.1371/journal.pone.0124633.